Basrah Journal for Engineering Sciences, Vol. 24, No. 1, (2024), 81-89

Original Article

Journal homepage: www.bjes.edu.iq
ISSN (Online): 23118385, ISSN (Print): 18146120

A Numerical Study of Blade Geometry Effects in a Vertical-Axes Wind Turbines

G. Omer-Alsultan [1, *], Ahmad A. Alsahlani [2]

[1,2] *Department of Mechanical Engineering, College of Engineering, University of Basrah, Basrah, Iraq*
E-mail addresses: omer.ghassan.abdulkareem@gmail.com , ahmad.mahdi@uobasrah.edu.iq
Received: 9 November 2023; Revised: 25 December 2023; Accepted: 7 January 2024; Published: 15 February 2024

Abstract

Several geometrical elements influence the aerodynamic properties of the Darrieus vertical axis wind turbines (VAWTs). Many extant studies have examined properties, such as solidity, pitching axis position (*x*/c), length of chord (c), blade quantity (N), diameter (d) of the rotor, and aspect ratio. However, not many have examined the shape of the airfoil (AF), which is a vital property that remains to be thoroughly investigated. Therefore, this present study used computational fluid dynamics (CFD) to investigate many airfoils blade characteristics, such as blade thickness (BT), maximum camber ratio (MCR), MCR location (MCRL), and air speed (AS), to determine their impact on VAWT performance. The results demonstrate a blade thickness BT of 10 to 12%, MCR of 0 to 22%, and MCRL of 24 to 23% yield a comparatively high coefficient of power, adequate optimal blade rotation to airspeed ratio (TSR), broader operational area, and high band efficiency while air velocities of 15 to 10% yield a comparatively higher power coefficient.

Keywords: Carbon dioxide-emission, Wind turbine, CFD, Savonius, H-Darrieus.

https://doi.org/10.33971/bjes.24.1.9

1. Introduction

Over the past few years, the energy-intensive lifestyles of humans as well as technological and industrial development have necessitated the emergence of new techniques with which to fulfil ever-increasing energy demands [1]. The decline in the availability of fossil fuels has only served to increase the cost of fuel. Furthermore, global warming as a result of the substantial amount of carbon dioxide (CO_2) emitted by fossil fuel use has also become a significant worry [2, 3]. The United States (U.S.) Energy Information Administration (2016) report predicts that global energy-linked CO_2 emissions will to rise from 32.3 billion metric tonnes in 2012 to 35.6 billion metric tonnes in 2020 and crest 43.2 billion metric tonnes by 2040 [4,5]. The developing world, which mainly relies on fossil fuels to satisfy its escalating energy demands, is mostly responsible for the recent rise in CO_2 emissions. Meanwhile, the amount of CO_2 emitted by countries that are not a part of the Organisation for Economic Co-operation and Development (OECD) are projected to reach ≈ 29.4 billion metric tonnes by 2040, which is 51% more than they emitted in 2012, while that of OECD countries are predicted to crest ≈13.8 billion metric tonnes; 8% higher than in 2012 (U.S. Energy Information Administration, 2016). As such, energy sources that are dependable, effective, eco-friendly, and long-lasting have garnered a lot of scientific interest in recent years [6].

The wind-based power generation capability was revised and increase by 143 gigawatts (GW) between 2023 to 2030, which is a 13% year-over-year (YOY) increase. However, this new YOY increase will only satisfy 68% of the wind-based power generation capability necessary to achieve the net-zero commitment to keep global warming to no more than 1.5°C. Nonetheless, the Global Wind Energy Council (GWEC) predicts that, so long as governments across the globe continue to adopt and enforce novel policies that enable the international supply chain to satisfy rising energy demands from both new and conventional markets as well as tackle issues; such as market design and permit issuance; the 2-terawatt (TW) milestone will be accomplished prior to 2030. However, to satisfy the Paris Agreement's objectives, the growth of wind-based power generation capability has to be increased by four times.

Wind turbines (WTs) are categorised as either vertical axis wind turbines (VAWTs) or horizontal axis wind turbines (HAWTs). The latter is commonly employed to convert medium to large amounts of energy as it is more efficient and compatible with extant energy grids [7, 8] while the former is popularly used to convert small to medium amounts of energy off the grid as it is easy to install and maintain, self-starts more effectively, only requires a small area to install, can capture multidirectional wind, does not require a yaw apparatus, is easy to fabricate, and does not produce much noise. Lift-based Darrieus WTs and drag-based Savonius rotors are two types of VAWTs [9, 10]. H-Darrieus WTs (HDWTs) are more efficient and have a broader tip speed ratio (TSR) than Savonius WTs [11]. There has been an uptick in the number of VAWTs installed at railroad lines, road medians, and high-rise edifices in both urban and rural locations to capture wind with medium to high air speeds (AS) and produce energy [12-14]. Nevertheless, this strategy cannot be adopted by locations that experience AS and sporadic winds annually as it would not be economical.

Savonius WTs are a type of VWAT that rely on inter-bucket differential drag to operate. Although this means that they can be used in locations that experience low AS, they are

still significantly inefficient [15, 16]. Darrieus WTs, however, are lift-based apparatus that yield better energy performance than Savonius WTs. Multiple studies have numerically and experimentally examined the performance and flow parameters of WTs to improve their efficiency and applicability [17]. Some of the more popular numerical simulations include the multiple stream tube (MST) model, the Vortex model, blade element momentum (BEM), and computational fluid dynamics (CFD) [18].

Analysis-based models; like Vortex [19, 20] and MST [21], use a one-dimensional (1D) simplified equation that solely relies on the drag and lift coefficients data measured at the air foil (AF). As such, they do not use wake data and solely use semi-empirical equations to predict dynamic stalls and examine tip vortices. Furthermore, as analysis-based models rely on AF data generated in static conditions, they fail to correctly predict when the AF will dynamically stall [22]. As CFD yields WT flow data that is more accurate than other numerical models, it is commonly used in wind energy research to develop more productive and effective WTs as well as to investigate, develop, and enhance WT blades.

To maximise output power and bending stiffness, Tavernier et al. [23] optimised the blade section of a variable pitch VAWT using a multi-objective evolutionary algorithm. Their simulation, which made use of the actuator cylinder approach and a vortex-based computer code, demonstrated the vital role that an optimal airfoil plays in boosting power generation for variable pitch VAWTs. In contrast, Li et al. [24] used the Genetic algorithm in conjunction with a two-dimensional CFD technique to discover the optimal pitch profile for a VAWT based on a power performance index. Their study showed how VAWT power performance may be effectively increased by changing pitch techniques.

Increasing Aspect Ratio (AR) effectively increases VAWT power output without sacrificing other aerodynamic design factors, as early Sandia research [25] shown. Blade ARs and Turbine ARs, which are contrasted below, are both included in AR. According to studies by Peng [26], Zanforlin [27], and Jain [28], increasing Turbine AR improves efficiency, Peng even demonstrates probable 100 percent improvements. According to Gosselin [29] and Hand [30], increasing Blade AR and efficiency are strongly associated. Nonetheless, their conclusions differ: Hand suggests minimal Cp rises above AR=10, but Gosselin finds a considerable difference between AR=7 and AR=15. Variations are most likely the consequence of unexplained variables influencing findings. It is recommended to maximize Blade and Turbine AR, although this should be done in conjunction with other design concerns. Low turbine AR affects wake velocity recovery, which has an influence on array design decisions, according to Hezaveh's [31] VAWT wake research. Furthermore, Xu et al. [32] used the semi-empirical double multiple stream tube to optimise the power output of a high-solidity variable pitch VAWT. The results of the post-optimization testing revealed that the VAWT's power performance increased by up to 78 %. Similarly, Peng et al. outperformed a fixed-pitch VAWT by determining the best variable pitch profile for a high-solidity VAWT [33, 34].

Therefore, this present study compares the aerodynamic performance of a tri-blade H-Darrieus and a 4-digit National Advisory Committee for Aeronautics (NACA) AF by examining their maximum AF blade thickness (BT), maximum camber ratio (MCR), and MCR location (MCRL) in NACA XX12 profiles [35]. Figure 3 depicts the shapes of the AFs, which helped assess the performance of VWATs based on the aerodynamic properties of several air speed, different Reynolds numbers (5 m/s, Re = 96965), (8 m/s Re = 155145), (10 m/s Re = 193931), (12 m/s Re = 232717) and (15 m/s Re = 290897). A simple blade analysis was carried out to support the efficiency results [36].

The Turbine thrust coefficient, and the coefficient of power for a wind turbine, C_t and C_p, respectively, can be formally defined as below. Conventionally, the thrust coefficient C_t is defined in relations with the wind speed and swept area of the turbine's swept area such that:

$$C_t = \frac{T}{0.5\ \rho\ A\ R\ U_\infty^2} \tag{1}$$

where T: rotor instantaneous torque (N.m), ρ : air density (kg/m^3), A is the rotor swept area (m^2), R is rotor radius (m) and U_∞ is the unperturbed wind velocity at computational domain entrance (m/s).

The corresponding power coefficient is defined as

$$C_p = \frac{Pw}{0.5\ \rho\ A\ R\ U_\infty^3} \tag{2}$$

where: Pw is the power of the passing air through the swept area and can be defined as:

$$Pw = \frac{1}{2}\ \rho U_\infty^3 A \tag{3}$$

As the wind turbine is spinning, the air velocity passing the blade is depending on the rotating speed as well as the wind speed. The ratio of the linear speed of spinning to the wind speed is defined as (TSR):

$$TSR = \frac{\omega R}{U_\infty} \tag{4}$$

ω : rotor angular velocity (rad/s).

Once TSR has been chosen, the geometry of the VAWT can be defined through a dimensionless parameter known as the solidity (σ) [37]:

$$\sigma = \frac{Nc}{2R} \tag{5}$$

where: N: number of rotor blades, c is the blade width (chord)

2. Model Descriptions

The examined rotor consisted of the blades with 4-digit NACA AF cross-sections that rotated in a counter-clockwise direction. Table 1 shows the primary geometry of a WT. The model would be examined with 2-D CFD analysis with Ansys Fluent. As presented in Fig. 1, the primary AF blade geometries; which included the BT, MCRL, and MCR, were examined. Furthermore, the effects of AS were also investigated.

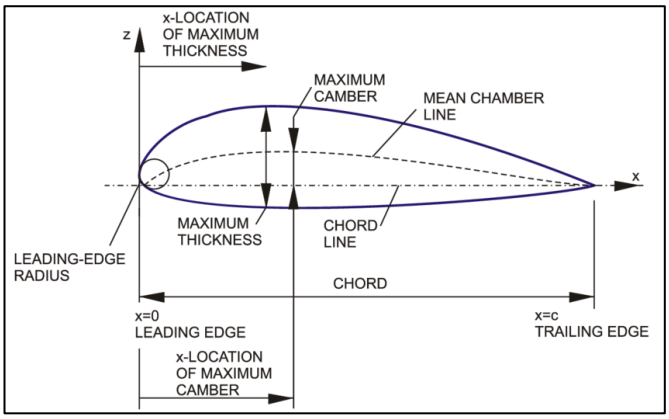

Fig. 1 Typical airfoil geometry.

The first digit (A) of the NACA 4-digit coding system, NACA ABXX, relates to the MCR of the average AF center line, whereas the second digit (B) corresponds to the MCRL. The final two digits represent the maximum BT. If A and B are both equal to 0, the AF is symmetric. The AFs investigated in this present study are listed in the table below. The first digit (A) of the NACA 4-digit coding system, NACA ABXX, relates to the MCR of the average AF center line, whereas the second digit (B) corresponds to the MCRL. The final two digits represent the maximum BT. If A and B are both equal to 0, the AF is symmetric. The AFs investigated in this present study are listed in the table below.

Table 1. The Studied airfoils parameters.

Thickness Study			
NACA	**Thickness ratio**	**Max. camber Ratio**	**Location of the max. camber ratio**
0010	10 %	0	Not Required
0012	12 %	0	Not Required
0015	15 %	0	Not Required
0018	18 %	0	Not Required
Maximum Camber Ratio Study			
0012	12 %	0 %	Not Required
2212	12 %	20 %	20 %
3212	12 %	30 %	20 %
4212	12%	40 %	20 %
The Location of Maximum Camber Ratio Study			
2212	12 %	20 %	20 %
2312	12 %	20 %	30 %
2412	12 %	20 %	40 %

3. NACA 4-digit airfoil calculation

The NACA airfoil section can be described using equations developed by National Advisory Committee for Aeronautics (NACA). The airfoil y-coordinate (yc) of the mean camber line can be generated using the defined maximum camber location (p) and its maximum camber ratio (m). The thickness distribution values (yt) also can be defined at given x-coordinate and given maximum thickness value (t):

Front ($0 \le x < p$)

$$y_c = \frac{m}{p^2}\,(2Px - x^2)$$

$$\frac{dy_c}{dx} = \frac{2M}{p^2}(P - x)$$

Back ($p \le x \le 1$)

$$y_c = \frac{M}{(1-P)^2}\,(1 - 2P + 2Px - x^2)$$

$$\frac{dy_C}{dx} = \frac{2M}{(1-P)^2}(P - x)$$

$$y_t = \frac{t}{0.2}(a_0 x^{0.5} + a_1 x + a_2 x^2 + a_3 x^3 + a_4 x^4) \qquad (6)$$

where:
$a_0 = 0.2969$, $a_1 = -0.126$, $a_3 = 0.2843$, $a_4 = -0.1015$ or -0.1036 for a closed trailing edge.

The x and y coordinates can be calculated using the coordinate of the mean camber line plus the thickness distribution.

Table 2. Main geometrical features of the tested model.

Blade profile	Symbol	Values
Chord	c	0.1 m
Diameter rotor	D	1.2 m
High rotor	H	1 m
Rotor swept area	As	1.2 m
Blade Length	L	1 m
Rotor solidity	σ	0.5
Number of blades	N	3
Free stream velocity	U_∞	5, 8, 10, 12, 15 m/s
Density of air,	ρ	1.225 kgm^{-3}
Turbulence model		SST $k-\omega$

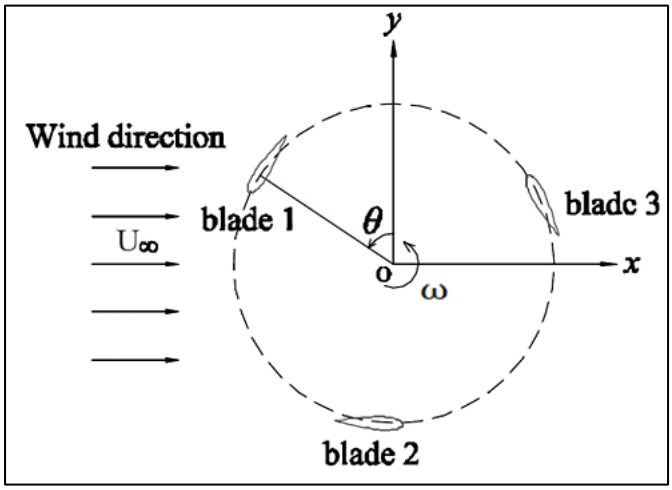

Fig. 2 Azimuthal coordinate of the vertical axis wind turbine.

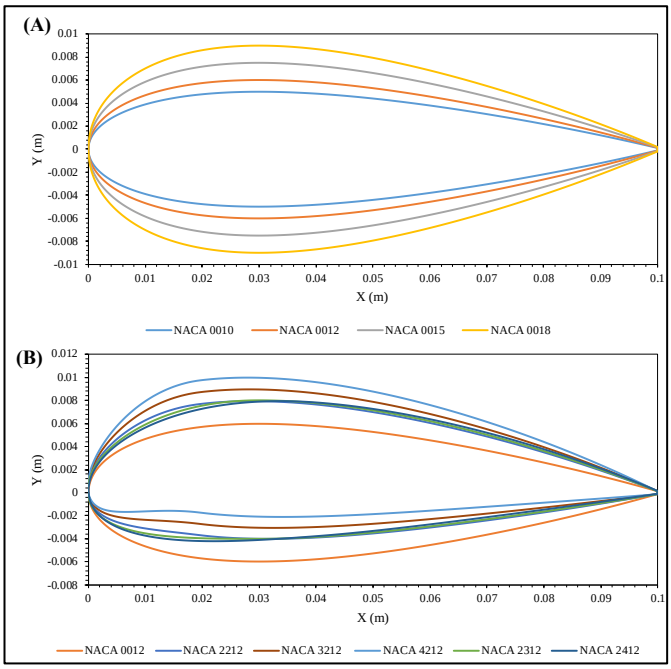

Fig. 3 Four-digit NACA airfoils: (A) symmetrical NACA series; (B) cambered airfoils.

4. Computational fluid dynamics (CFD) modelling

Figure 4 presents the computational domain, wherein the boundaries were adequately far away from the rotor for minimising boundary effects like blockage conditions and insufficient wake development. The rotor displays a diameter (*d*) of 1.2 m while the length of chord (*c*) was 0.1 m. The researchers established the upwind and side boundaries as equivalent to 4d from the VAWT axis whereas the downwind boundary was 10d away. The domain includes 1 stationary, outer sub-domain and one rotating, inner sub-domain. The above sub-domains show an interface of 16c from the VAWT blades [38].

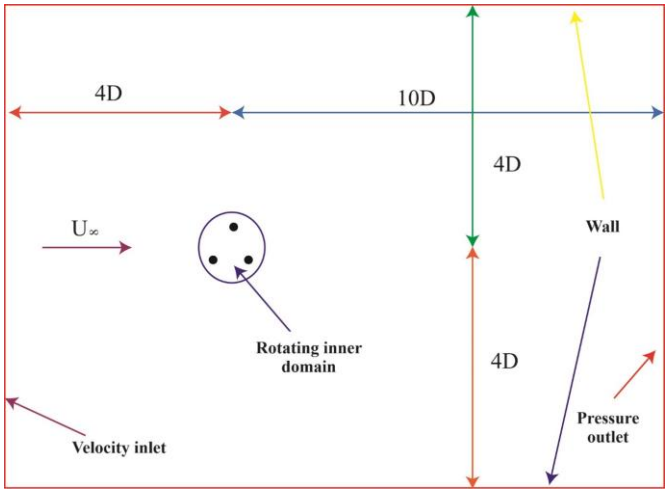

Fig. 4 Details of the 2D CFD model for a single VAWT blade computational domain.

The Ansys Fluent® module was used to do the CFD analysis of the VAWT. Triangular-type mesh elements with 97150 nodes and 127697 elements were employed for meshing since they are appropriate for two-dimensional (2-D) models [39]. The mesh near the VAWT could be used for improving the precision near the WT blades, as shown in Fig. 5, hence the smallest element size of 0.05 m was utilised [39]. A broad domain was chosen to ensure smooth flow conditions and to reduce the disruption caused by backflow from the wall. Here, a growth rate of 1.20 was used.

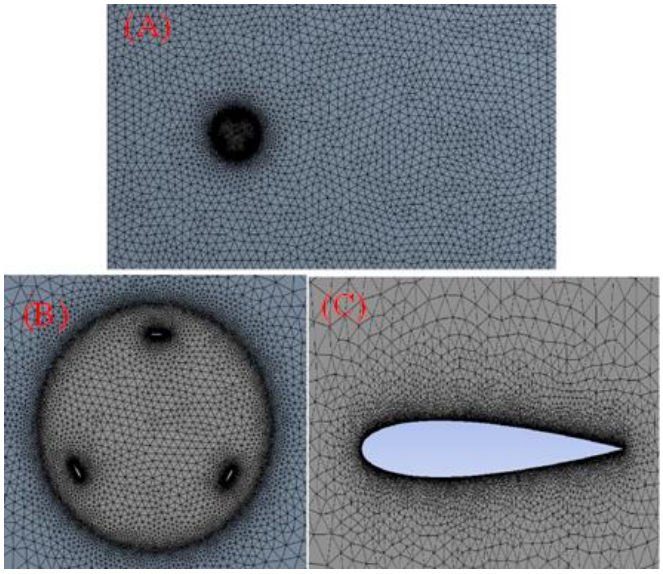

Fig. 5 (A) Mash domain (B) Mash rotor (C) Mash airfoil.

5. Results and discussion

5.1. Blade thickness (BT)

Many symmetrical AFs of varying BTs using four NACA profiles; namely, 0010, 0012, 0015, and 0018, were examined. The *c*, blade quantity (*N*), and pitching axis position (*x/c*) were fixed at 0.1, 3, and 0.1, respectively. As illustrated in Fig. 6, the WT's power coefficient was determined for each example at varying TSRs. The results suggest that the maximal power coefficient was achieved at a TSR of ≈ 3. However, with an increase in the BT and TSR, it was noted that drag forces exceeded the resulting torque, reducing the TSR range at which it delivered functional torque.

Figure 6 also depicts the power coefficient fluctuations with regards to TSR for rotors with varying maximum BTs. The findings seen in Fig. 6 indicate that the C_p initially increased to a maximal value and eventually decreased with increasing TSR for all the rotors. The maximum C_p increased with increasing the maximum BT if the maximum BT was < 12%, and it increased with a reduction in the maximum BT if the maximum BT was > 12%. The C_p for NACA 0010, NACA 0012, NACA 0015, and NACA 0018 were 0.526, 0.504, 0.499, and 0.467, respectively. The power coefficient shows the following trend, i.e., $C_{p\ NACA\ 0012} > C_{p\ NACA\ 0010} > C_{p\ NACA\ 0015} > C_{p\ NACA\ 0018}$, when the values decreased below the optimal TSR, whereas it increased with decreasing the maximum BT above the optimal TSR. As the maximum BT decreased, the optimal TSR and operational zone increased. These results imply that the smaller the angular speed required to produce the highest power output, the thinner the BT must be. The rotors with the NACA 0012 and NACA 0010 AFs generated wider high-efficiency bands. According to the aforementioned findings, the optimal maximum BT was 12 to 10%.

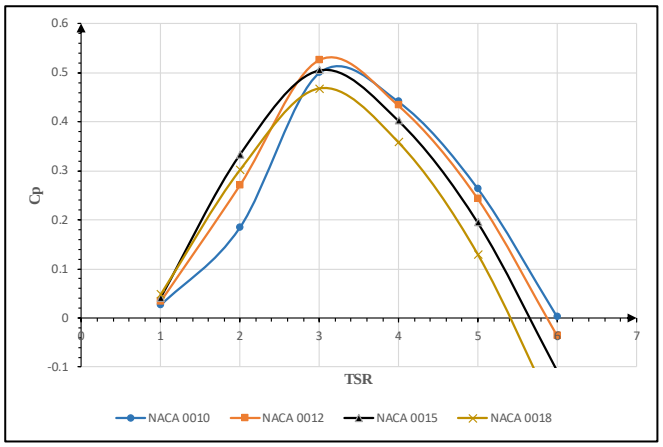

Fig. 6 Symmetric airfoils NACA-4 Digit performance plots: Power coefficient (Cp) versus tip speed ratio (TSR).

Figure 7 depicts the torque coefficient of rotor blades for a single cycle (0-360 degrees) at TSR = 3. The results show that NACA0012 has a higher torque coefficient, which has resulted in a higher power coefficient. It may be concluded that increasing the BT at this speed restriction could harm the WT's performance, which may have occurred owing to flow separation at a specified thickness and has resulted in increased drag forces.

The results in Fig. 7 also demonstrate that every curve is repeated at every 120° as the current WT has three blades. It was noted that the C_m was > 0 for nearly every rotational period. The maximal instantaneous torque coefficients were seen to be positioned near the points with θ = 100°, 220°, and 340°, and 0.181, 0.185, 0.179, and 0.165 for the NACA 0010, NACA 0012, NACA 0015, and NACA 0018 models, respectively. On the other hand, the minimal instantaneous torque coefficients were seen to be positioned near θ = 45°, 160°, and 280° and 0.06, 0.065, 0.062, and 0.06 for the NACA 0010, NACA 0012, NACA 0015, and NACA 0018 models, respectively. To conclude, the NACA 0012 and NACA 0015 models exhibit the best and worst torque characteristics, respectively.

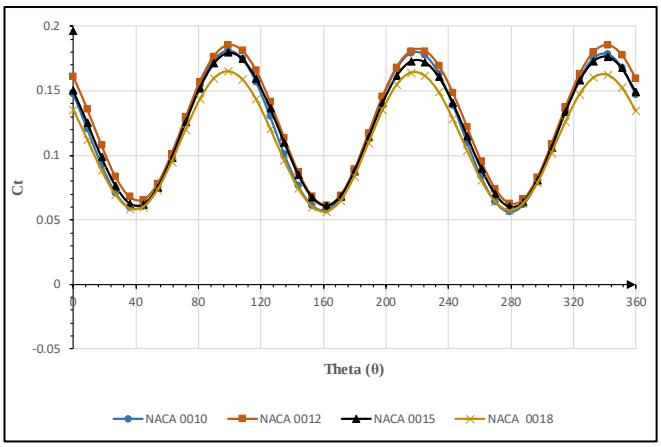

Fig. 7 Symmetric airfoil performance plots: Torque coefficient curves versus Theta at TSR = 3.

5.2. Maximum camber ratio (MCR)

In this present study, many symmetrical AFs with varied MCRs using 4 NACA profiles; namely, 0012, 2212, 3212, and 4212, were examined. The WT's power coefficient was computed for each example at varying speed ratios (TSR), as illustrated in Fig. 8. The results suggested that the highest power coefficient was attained at a TSR of roughly 3 for NACA 0012, 2212, 3212, and NACA 4212 at a TSR of 4. However, with an increase in the MCR and the high-TSR, it was noted that drag forces exceeded the produced torque, which further decreased the TSR range at which it produced effective torque.

Figure 8 also depicts the fluctuation in power coefficient with regards to TSR for rotors with varying MCRs. Figure 7 illustrates that for all rotors, C_p initially increased to a maximal value, and then decreased with increasing TSR. An increase in the MCR led to a decrease in the maximal C_p when the MCR was < 12%. The power coefficient showed the following trend; i.e., $C_{p\ NACA\ 0012} > C_{p\ NACA\ 3212} > C_{p\ NACA\ 2212} > C_{p\ NACA\ 4212}$; when the MCR was below the optimal TSR, whereas it increased when the MCR decreased below the optimal TSR. The results further indicated that the optimal TSR and operational zone increased with decreasing MCR. The rotors with NACA 0012 and NACA 3212 AFs exhibited wide high efficiency bands. Furthermore, the findings showed that the majority of the effective MCR ranged between 0 and 22%.

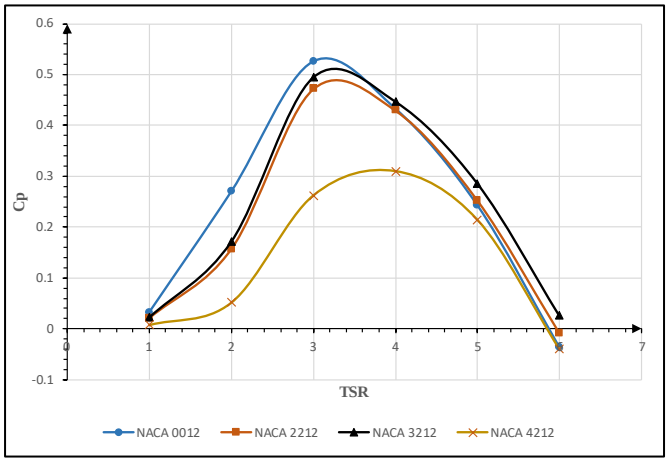

Fig. 8 Wind turbine performance using different airfoils with different maximum camber ratio.

Figure 9 depicts the torque coefficient of all blades at TSR = 3 for NACA (0012, 2212, 3212) and NACA 4212, where the TSR was 4 for a single cycle (0-360 degrees). NACA0012 showed a higher torque coefficient, which led to a higher power coefficient. It may be concluded that an increase in the MCR of blades at this speed limit could impair WT performance, which may have occurred owing to flow separation at a particular MCR. This further led to an increase in drag forces.

Furthermore, the results in Fig. 9 indicate that every curve was repeated after 120°. This could be attributed to the fact that the existing WT contain three blades. It was noted that the C_T was > 0 during the complete rotational period. The maximal instantaneous torque coefficients were seen to be positioned near θ = 100°, 220°, and 341° and were 0.0185, 0.175, 0.174, and 0.115 for the NACA 0012, NACA 2212, NACA 3212, and NACA 4212 models, respectively. The minimal instantaneous torque coefficients were seen to be positioned near θ = 35°, 155°, and 275° and 0.065, 0.056, 0.0641, and -0.0058 for the NACA 0012, NACA 2212, NACA 3212, and NACA 4212 models, respectively. To conclude, the NACA 0012 and NACA 4212 models presented the best and worst torque characteristics.

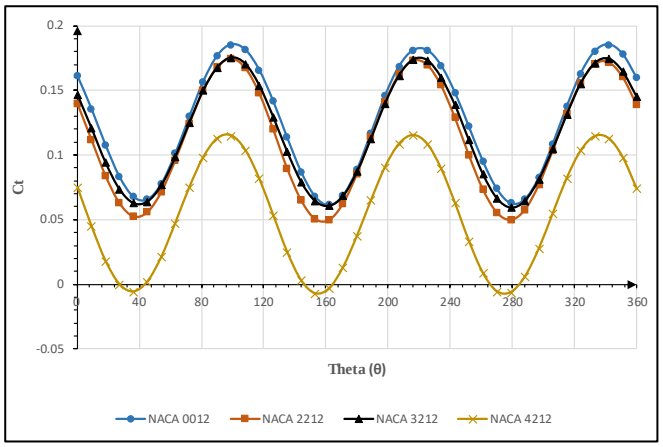

Fig. 9 Torque coefficient curves versus rotating angle at TSR = 3 for the NACA (0012, 2212, 3212) and NACA 4212 at TSR = 4.

5.3. Maximum camber ratio location (MCRL)

Four NACA profiles, namely 2212, 2312, and 2412, were used to study a number of AFs with varying MCRLs for the WTs. As illustrated in Fig. 10, the WT's power coefficient was determined for each example at various TSR. The results demonstrate that at a TSR of roughly 3, the maximal power coefficient was attained. However, when the MCRL for the WTs was increased at a higher TSR, it was noted that drag forces overcame the torque, and decreased the TSR range at which effective torque was generated.

In addition, Fig. 10 depicts the fluctuations in the power coefficient with regard to TSR for WT rotors with varied MCRL. As seen in Fig. 10, for all rotors, C_p initially increased to a maximal value and eventually decreased with increasing TSR. It was further noted that when the MCRL was < 24%, there was an increase in the maximal C_p. However, when the MCRL was > 22%, a decrease in maximal C_p was seen. The following power coefficient trend was noted: $C_{p\ NACA\ 2412} > C_{p\ NACA\ 3212} > C_{p\ NACA\ 2212}$. The results further showed an increase in optimal TSR and operational zone when the MCRL decreased. The rotors with NACA 2412 and NACA 2312 AFs showed wide high-efficiency bands. The above-mentioned findings showed that the effective MCRL was 24 to 23%.

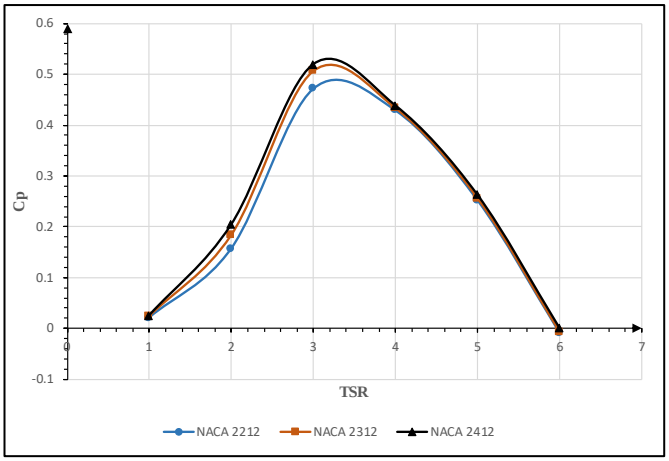

Fig. 10 Symmetric airfoils NACA-4 digit performance plots: Power coefficient (CP) versus tip speed ratio (TSR).

Figure 11 depicts the torque coefficient of rotor blades for one cycle (0-360 degrees) at TSR = 3. The results show that NACA 2412 displays a higher torque coefficient, which has resulted in an improved power coefficient. It may be concluded that an increase in the MCRL of the blades at this speed limit would affect the WT performance, which may have occurred owing to flow separation at particular MCRLs, resulting in increased drag forces.

The findings in the figure also indicate that every curve repeat at every 120°. This could be attributed to the fact that the existing WT has three blades. The C_T was seen to be > 0 during the complete rotational period. The maximal instantaneous torque coefficients were positioned near θ = 100°, 220°, and 340° and 0.170, 0.177, and 0.178 for the NACA 2212, NACA 2312, and NACA 2412 models, respectively. The minimal instantaneous torque coefficients were positioned near θ = 40°, 160°, and 280° and 0.056, 0.064, and 0.066 for the NACA 2212, NACA 2312, and NACA 2412 models, respectively. To conclude, the NACA 2412 and NACA 2212 models displayed the best and worst torque characteristics.

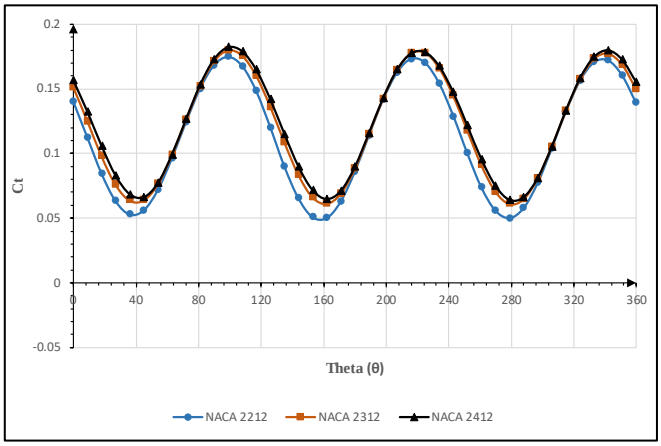

Fig. 11 Symmetric airfoil performance plots: Torque coefficient curves and Theta at TSR 3.

5.4. Effect of changes in air speed (AS)

In the past, researchers have determined the influence of AS on a symmetrical AF. The WT's power coefficient was estimated at varying TSR for each example Fig. 12, which indicates the fluctuation in power coefficient with regard to TSR for rotors at varying AS. The findings show that elevating the AS increases the WT's power coefficient, which is observed in all of the examined blades. The power coefficient vs. TSR pattern shows a similar trend, and as previously stated, the maximal C_p increased with an increase in AS. The C_p were 0.452, 0.483, 0.499, 0.514, and 0.533 for AS of 5, 8, 10, 12, and 15 m/s, respectively. The power coefficient shows the following trend, i.e., C_p AS 15 > C_p AS 12 > C_p AS 10 > C_p AS 8 > C_p AS 5, when the value was lower than the optimal TSR, whereas it increased with a decrease in the maximal BT beyond the optimal TSR. The rotors with AS of 15 m/s and 12 m/s exhibited wide higher efficiency bands. The above findings implied that the effective AS was between 10 and 15.

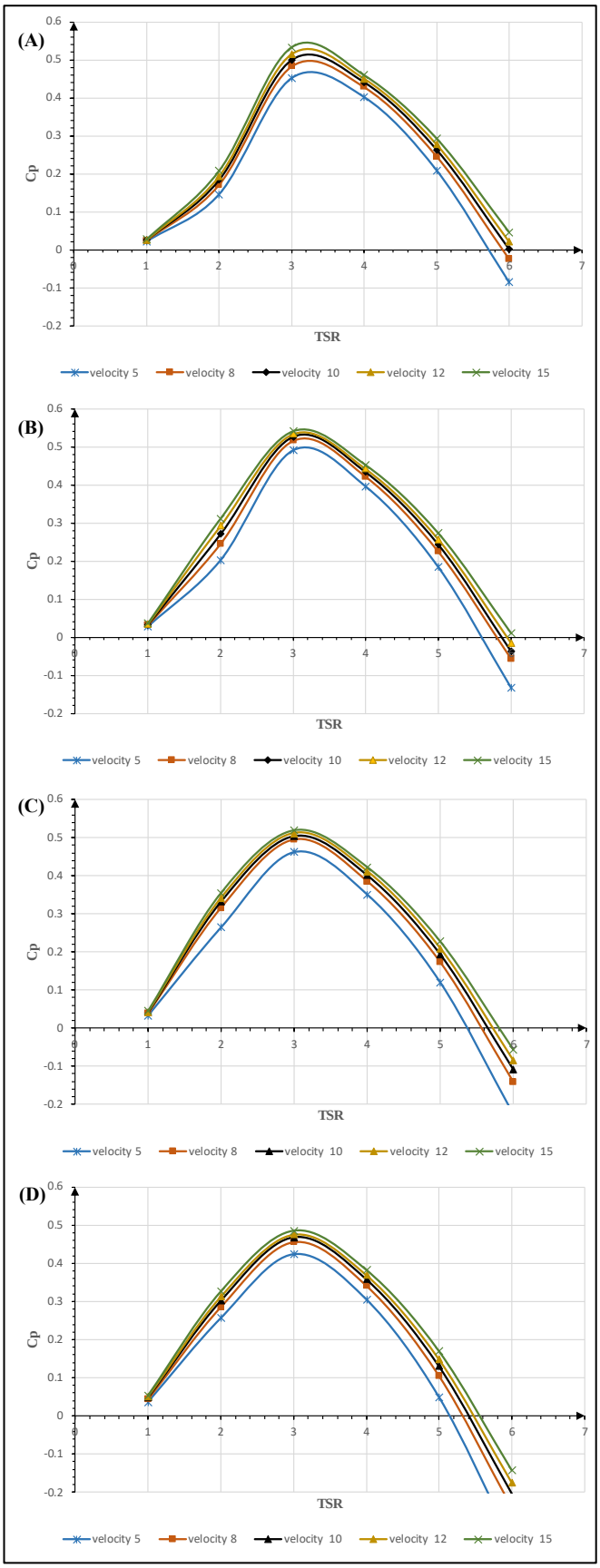

Fig. 12 Symmetric airfoils (A) NACA 0010 (B) NACA 0012 (C) NACA 0015 (D) NACA 0018 performance plots: Power coefficient (Cp) versus tip speed ratio (TSR).

Conclusions

Here, the performance of a vertical WT has been evaluated in relation to the effects of MCR, BT, MCRL, and AS. The researchers also compared the power coefficient and torque coefficient for the single blade and rotors at varying azimuth angles. The major results of the present study have been summarised below:

1. Except for one case where the MCR was pushed towards the trailing edge of the blade, the studied cases showed that the maximal power coefficient was reached at TSR = 3.
2. The BT also displays a significant effect on WT performance and it was noted that an optimal BT improved the power coefficient. The results showed that out of all the cases, the effective BT was seen to range from 10 to 12%.
3. It was seen that a shift in the MCRL towards the trailing edge beyond 22% of the blade could affect WT efficiency.
4. The findings implied that the AS improved the WT efficiency and was attributed to improved flow characteristics that could produce additional torque.

Several alternative H-type VAWTs of various sizes and AS could be constructed and evaluated with the VAWT computation and analysis techniques. However, in the future, the researchers will conduct an in-depth examination to confirm that the above conclusions may be applied in different systems. Furthermore, wind tunnel experiments will be undertaken and the experimental data will be compared to the computational findings. In addition, more research can be conducted with CFD models and wind tunnel tests to determine the effect of additional AF parameters, like the leading-edge radius and the BT and angle of the trailing edge. This could significantly improve the AF design of Darrieus VAWTs.

References

[1] S. Roy, A. Ducoin, “Unsteady analysis on the instantaneous forces and moment arms acting on a novel Savonius-style wind turbine”, Energy Convers Management, vol. 121, pp. 281-296, 2016. https://doi.org/10.1016/j.enconman.2016.05.044

[2] G. Abdulkareem-Alsultan, N. Asikin-Mijan, L. K. Obeas, R. Yunus, S. Z. Razali, A. Islam, Y. H. Taufiq-Yap, “In-situ operando and ex-situ study on light hydrocarbon-like-diesel and catalyst deactivation kinetic and mechanism study during deoxygenation of sludge oil”, Chemical Engineering Journal, vol. 249, 2022. https://doi.org/10.1016/j.cej.2021.132206

[3] G. Abdulkareem-Alsultan, N. Asikin-Mijan, Y. H. Taufiq-Yap, “Effective catalytic deoxygenation of waste cooking oil over nanorods activated carbon supported CaO”, Key Engineering Materials, vol. 707, pp. 175-181, 2016. https://doi.org/10.4028/www.scientific.net/KEM.707.175

[4] N. Asikin-Mijan, G. AbdulKareem-Alsultan, M.S. Mastuli, A. Salmiaton, M. A. Mohamed, H. V. Lee, Y. H. Taufiq-Yap, “Single-step catalytic deoxygenation-cracking of tung oil to bio-jet fuel over CoW/silica-alumina catalysts,” Fuel, vol. 325, p. 124917, Oct. 2022. https://doi.org/10.1016/j.fuel.2022.124917

[5] Y. Zhang, W. Chen, and W. Gao, "A survey on the development status and challenges of smart grids in main driver countries," Renewable and Sustainable Energy Reviews, vol. 79, pp. 137–147, Nov. 2017. https://doi.org/10.1016/j.rser.2017.05.032

[6] A. Kibria, S. B. Akhundjanov, and R. Oladi, "Fossil fuel share in the energy mix and economic growth," International Review of Economics & Finance, vol. 59, pp. 253–264, Jan. 2019. https://doi.org/10.1016/j.iref.2018.09.002

[7] B. Desalegn, D. Gebeyehu, and B. Tamirat, "Wind energy conversion technologies and engineering approaches to enhancing wind power generation: A review," Heliyon, vol. 8, no. 11, p. e11263, Nov. 2022. https://doi.org/10.1016/j.heliyon.2022.e11263

[8] K. B. Tawfiq, A. S. Mansour, H. S. Ramadan, M. Becherif, and E. E. El-kholy, "Wind Energy Conversion System Topologies and Converters: Comparative Review," Energy Procedia, vol. 162, pp. 38–47, Apr. 2019. https://doi.org/10.1016/j.egypro.2019.04.005

[9] S. Roga, S. Bardhan, Y. Kumar, and S. K. Dubey, "Recent technology and challenges of wind energy generation: A review," Sustainable Energy Technologies and Assessments, vol. 52, p. 102239, Aug. 2022. https://doi.org/10.1016/j.seta.2022.102239

[10] M. Ahmad, A. Shahzad, and M. N. M. Qadri, "An overview of aerodynamic performance analysis of vertical axis wind turbines," Energy & Environment, p. 0958305X2211212, Aug. 2022. https://doi.org/10.1177/0958305x221121281

[11] A. Hosseini and N. Goudarzi, "Design and CFD study of a hybrid vertical-axis wind turbine by employing a combined Bach-type and H-Darrieus rotor systems," Energy Conversion and Management, vol. 189, pp. 49-59, 2019. https://doi.org/10.1016/j.enconman.2019.03.068

[12] E. Singh, S. Roy, Yam Ke San, Ming Chiat Law, and Perumal Senthil Kumar, "Computational Analysis of Air Energy Extractors for Guided Flow Exhaust Applications," pp. 185–204, Sep. 2022. https://doi.org/10.1007/978-981-19-2412-5_11

[13] E. Singh, S. Roy, Ke San Yam, and Ming Chiat Law, "Numerical analysis of H-Darrieus vertical axis wind turbines with varying aspect ratios for exhaust energy extractions," Energy, vol. 277, pp. 127739–127739, Aug. 2023. https://doi.org/10.1016/j.energy.2023.127739

[14] E. Singh, S. Roy, and Y. Ke San, "Numerical Analysis of Exhaust Air Energy Extractor for Cooling Tower Applications," IOP Conference Series: Materials Science and Engineering, vol. 943, p. 012035, Nov. 2020. https://doi.org/10.1088/1757-899x/943/1/012035

[15] V. Vishnu Namboodiri and R. Goyal, "Benchmarking the darrieus wind turbine configurations through review and data envelopment analysis," Clean Technologies and Environmental Policy, vol. 25, no. 7, pp. 2123–2155, Jun. 2023. https://doi.org/10.1007/s10098-023-02554-8

[16] K. Venkatraman, S. Moreau, J. Christophe, and C. Schram, "Numerical investigation of h-Darrieus wind turbine aerodynamics at different tip speed ratios," International Journal of Numerical Methods for Heat & Fluid Flow, Mar. 2023. https://doi.org/10.1108/hff-09-2022-0562

[17] M. Ali et al., "Low profile wind savonius turbine triboelectric nanogenerator for powering small electronics," Sensors and Actuators A: Physical, vol. 363, p. 114535, Dec. 2023. https://doi.org/10.1016/j.sna.2023.114535

[18] A. R. Sengupta, A. Biswas, and R. Gupta, "Studies of some high solidity symmetrical and unsymmetrical blade H-Darrieus rotors with respect to starting characteristics, dynamic performances and flow physics in low wind streams," Renewable Energy, vol. 93, pp. 536–547, Aug. 2016. https://doi.org/10.1016/j.renene.2016.03.029

[19] M. Pinsky, Eshkol Eytan, Ehud Gavze, and A. Khain, "Vortex Structure of Head Bubble in Convective Cloud Starting Plume," Journal of the Atmospheric Sciences, vol. 80, no. 8, pp. 2091–2113, Aug. 2023. https://doi.org/10.1175/jas-d-22-0122.1

[20] G. A. DiMaggio, R. J. Hartfield, and V. Ahuja, "Solid Rocket Motor Internal Ballistics Using a Vortex Particle Method," Jun. 2023. https://doi.org/10.2514/6.2023-4032

[21] A. G. Ajay, L. Morgan, Y. Wu, D. Bretos, A. Cascales, O. Pires, C. Ferreira, "Aerodynamic model comparison for an X-shaped vertical-axis wind turbine," Sep. 2023. https://doi.org/10.5194/wes-2023-115

[22] F. Geng, I. Kalkman, A. S. J. Suiker, and B. Blocken, "Sensitivity analysis of airfoil aerodynamics during pitching motion at a Reynolds number of 1.35×105," Journal of Wind Engineering and Industrial Aerodynamics, vol. 183, pp. 315–332, Dec. 2018. https://doi.org/10.1016/j.jweia.2018.11.009

[23] A. Nejad, Y. Guo, Z. Gao, and T. Moan, "Development of a 5 MW Reference Gearbox for Offshore Wind Turbines," Wind Energy, vol. 19, pp. 1089-1106, 2015. https://doi.org/10.1002/we.1884

[24] C. Li, Y. Xiao, Y. Xu, Y. Peng, G. Hu, and S. Zhu, "Optimization of blade pitch in H-rotor vertical axis wind turbines through computational fluid dynamics simulations," Applied Energy, vol. 212, pp. 1107–1125, Feb. 2018. https://doi.org/10.1016/j.apenergy.2017.12.035

[25] H. J. Sutherland, D. E. Berg, T. D. Ashwill, "A Retrospective of VAWT Technology", Security, pp. 1-64, 2012.

[26] P. Jain and A. Abhishek, "Performance prediction and fundamental understanding of small scale vertical axis wind turbine with variable amplitude blade pitching," Renewable Energy, vol. 97, pp. 97–113, Nov. 2016. https://doi.org/10.1016/j.renene.2016.05.056

[27] S. Zanforlin and S. Deluca, "Effects of the Reynolds number and the tip losses on the optimal aspect ratio of straight-bladed Vertical Axis Wind Turbines," Energy, vol. 148, pp. 179–195, Apr. 2018. https://doi.org/10.1016/j.energy.2018.01.132

[28] H. Y. Peng, H.-F. Lam, and H. J. Liu, "Power performance assessment of H-rotor vertical axis wind turbines with different aspect ratios in turbulent flows via experiments," Energy, vol. 173, pp. 121–132, Apr. 2019. https://doi.org/10.1016/j.energy.2019.01.140

[29] R. Gosselin, "Analysis and optimization of vertical axis turbines", Ph.D thesis, Mechanical Engineering, 2015.

[30] B. Hand and A. Cashman, "Conceptual design of a large-scale floating offshore vertical axis wind turbine," Energy Procedia, vol. 142, pp. 83–88, Dec. 2017. https://doi.org/10.1016/j.egypro.2017.12.014

[31] S. H. Hezaveh, E. Bou-Zeid, M. W. Lohry, and L. Martinelli, "Simulation and wake analysis of a single vertical axis wind turbine," Wind Energy, vol. 20, no. 4, pp. 713–730, Sep. 2016. https://doi.org/10.1002/we.2056
[32] Y.-L. Xu, Y.-X. Peng, and S. Zhan, "Optimal blade pitch function and control device for high-solidity straight-bladed vertical axis wind turbines," Applied Energy, vol. 242, pp. 1613–1625, May 2019. https://doi.org/10.1016/j.apenergy.2019.03.151
[33] I. Paraschivoiu, O. Trifu, and F. Saeed, "H-Darrieus Wind Turbine with Blade Pitch Control," International Journal of Rotating Machinery, vol. 2009, pp. 1–7, 2009. https://doi.org/10.1155/2009/505343
[34] Y.-X. Peng, Y.-L. Xu, and S. Zhan, "A hybrid DMST model for pitch optimization and performance assessment of high-solidity straight-bladed vertical axis wind turbines," Applied Energy, vol. 250, pp. 215–228, Sep. 2019. https://doi.org/10.1016/j.apenergy.2019.04.127
[35] K. Rogowski, M. O. L. Hansen, and G. Bangga, "Performance Analysis of a H-Darrieus Wind Turbine for a Series of 4-Digit NACA Airfoils," Energies, vol. 13, no. 12, p. 3196, 2020. https://doi.org/10.3390/en13123196
[36] A. Dumitrache, F. Frunzulica, H. Dumitrescu, and B. Suatean, "Influences of some parameters on the performance of a small vertical axis wind turbine," Renewable Energy and Environmental Sustainability, vol. 1, p. 16, 2016. https://doi.org/10.1051/rees/2016024
[37] T. J. Carrigan, B. H. Dennis, Z. X. Han, and B. P. Wang, "Aerodynamic Shape Optimization of a Vertical-Axis Wind Turbine Using Differential Evolution," ISRN Renewable Energy, vol. 2012, pp. 1–16, 2012. https://doi.org/10.5402/2012/528418
[38] L. A. Danao, N. Qin, and R. Howell, "A numerical study of blade thickness and camber effects on vertical axis wind turbines," Proceedings of the Institution of Mechanical Engineers, Part A: Journal of Power and Energy, vol. 226, no. 7, pp. 867–881, Jul. 2012. https://doi.org/10.1177/0957650912454403
[39] A. Loya, M. Z. U. Khan, R. A. Bhutta, and M. Saeed, "Dependency of Torque on Aerofoilcamber Variation in Vertical Axis Wind Turbine," World Journal of Mechanics, vol. 06, no. 11, pp. 472–486, 2016. https://doi.org/10.4236/wjm.2016.611033